Physical chemical properties of geomaterials

Bublikova T.M.[1], Balitsky V.S.[1], Nekrasov A.N.[1], Setkova T.V.[1], Krikunova P.V.[2], Mikhailova P.S.[2], Gavrilova E.O.[2]

Experimental investigation of the influence of the concentration of ammonia solutions on the sizes of malachite crystals in the mass crystallization process. UDC: 549.057:549.743.12:548.231.1

[1] IEM RAS, Chernogolovka (tmp@iem.ac.ru)

[2] Lomonosov Moscow State University, Moscow

Abstract. The morphology and structural features of aggregates of natural and synthetic malachite were studied by scanning electron microscopy. Synthetic malachite was obtained in ammonium hydroxide solutions of various concentrations: 0.2; 0.5; 2.0 and 2.5 m NH_4OH. It is shown that an increase in the concentration of ammonia in the solution leads to an increase in the crystallization rate and an increase in the size of the crystals that form malachite aggregates.

Keywords: malachite, synthesis, ammonia solutions, crystallization, evaporation-recirculation system, scanning electron microscopy, parallel-columnar aggregate, spherulites

Malachite is the basic copper carbonate, widely occurring mineral in the oxidation zone of sulfide copper and polymetallic deposits. He is one of the most popular ornamental stones, due to its bright color, variety of intricate texture patterns and good polishability. Unique products made from stone of the famous Ural Gumeshevsky and Mednorudyansky deposits, brought Russian malachite is widely known. The increased interest in malachite is due not only by its value as a jewelry and ornamental material. The attention of mineralogists and gemologists are attracted by the variety of forms of malachite formation, the presence of a large variety of its textures: radially radiant, rectilinear and wavy-banded textures, kidney-shaped concentric-zonal, patterned, breccia, etc., as well as combined texture, which is a combination of different textural malachite varieties. The individual malachite crystals are found very rarely.

The investigations of various texture types, color zoning of malachite, and origin of spherulites with an internal radial-radiant structure for many years were performed by D.P. Grigoriev (Grigoriev, 1953). The most comprehensive summarizing data on morphology, forms of isolation, history of development of malachite deposits is presented in monographs by V.B. Semenov (Semenov, 1987). The relationship between the gemological characteristics of malachite and the geological and geochemical characteristics of host rocks and their composition is described in detail in E. Mukendi work using the example of malachite from deposits of the Katanga copper ore belt (Central Africa) (Mukendi, 2009). Morphology aggregates of malachite and physicochemical properties of a synthetic analogue of natural malachite was studied at the IEM RAS, St. Petersburg State University, Moscow State Research Institute (Bublikova et al., 2019; Shuisky, 2015; Chernenko and Melnikov, 2003; J. Xu and D. Xue, 2005 and others).

The objective of this study was to study the morphology, structural features and sizes of aggregates of the synthetic malachite in comparison with the natural mineral. For the study, samples of malachite from the Kolwezi deposit (DR Congo) were used, as they are closest in texture to the synthetic malachite.

Synthetic malachite was obtained in recirculation-evaporation crystallizers according to the method developed by us at the IEM RAS (Bublikova, Balitsky et al., 2000). Two series of experiments were carried out. In the first series of experiments, low-concentration solutions of 0.2 and 0.5 m NH_4OH were used. Duration of experiments was 35 - 50 days. In the second series, concentrated crystallization solutions of 2.0 and 2.5 m NH_4OH were used for a duration experiments 20 - 30 days. Crystallization of malachite from solution occurred on a horizontal surface of the bottom of the crystallizer at a temperature of 65 to 80 ºC. In the experiments carried out at a constant temperature of crystallization obtained plush malachite with weakly expressed color zoning. Malachite banded texture with contrast zoning and alternation of shades from light to dark green obtained in experiments where the crystallization temperature was changed by 7 - 10 ºC every 5 - 7 days.

Samples of natural and synthesized malachite were studied under optical (MBS- 10), and polarizing (Nikon Eclipse LV100pol) microscopes. Morphology and internal the structure of the samples was studied on chips and polished surfaces of malachite samples using a scanning microscope Tescan Vega II XMU.

Synthetic malachite obtained in solutions of 0.2 m NH_4OH is composited by parallel columnar units. Malachite crystals have a prismatic habit, isometric, about 0.2–0.4 μm thick (Fig. 1a). Individual spherulites up to 400 microns in diameter, formed in the volume of the solution, have a radially radiant structure. The thickness of the overgrown layer is 450–500 μm. Because the source material (basic copper carbonate) has very low solubility in 0.2 m NH_4OH solutions (Bublikova et al. 2021.), then the saturation of the solution with copper occurs within several days. It was not possible to determine the beginning of the malachite crystallization process from a solution. Taking into account the thickness of the overgrown layer, it can be argued that the rate growth of malachite does not exceed 10 microns/day.

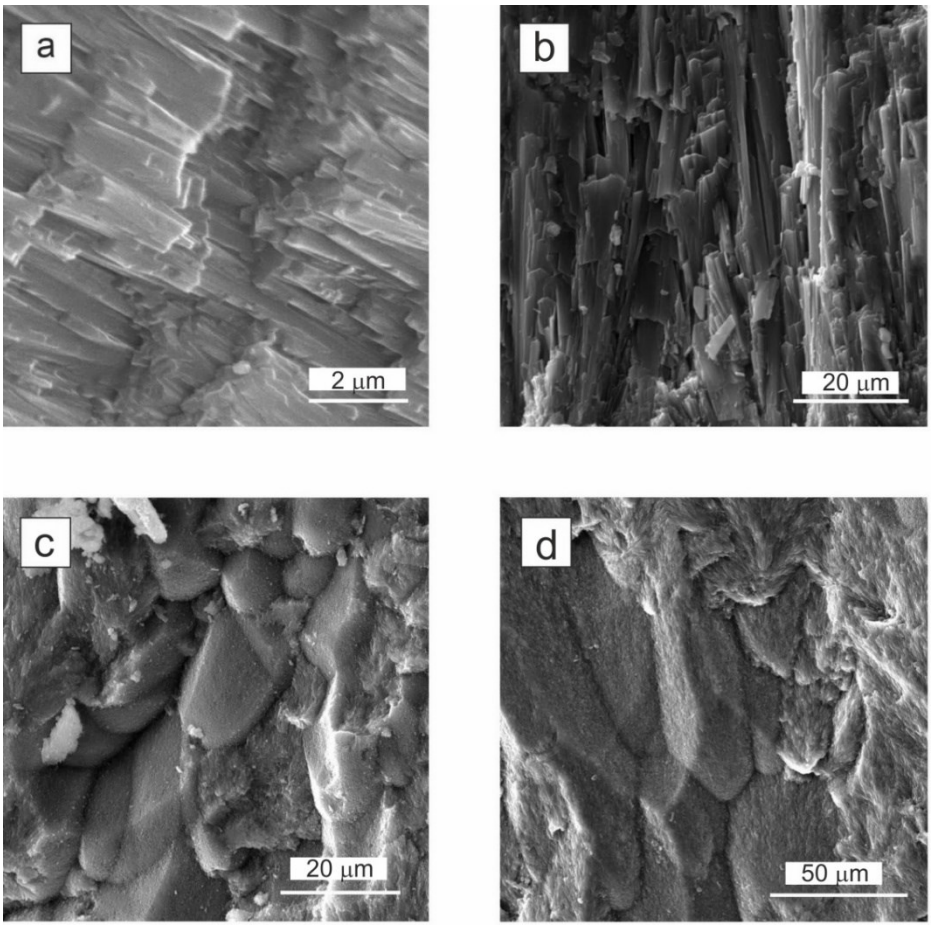

Fig.1 SEM images in secondary electrons of synthetic malachite samples, obtained using ammonium hydroxide solutions: a – 0.2 m; b – 0.5 m; c - 2.0 m; (d) 2.5 m NH4OH.

Malachite synthesized in 0.5 m NH_4OH solutions also consists of parallel- shear units. Crystals have a prismatic habit, elongated (Fig. 1b), crystal sizes are 4 - 8 microns thick. The crystallization rate of malachite varies from 10 to 15 microns/day.

Details of the structure of malachite obtained in experiments with solutions of 2.0 and 2.5 m NH_4OH are shown in Fig. 1 c, d. Synthetic malachite crystal sizes are 7 - 15 and 18 - 21 μm respectively. The crystallization rate of mineral aggregates in experiments with participation of 2.5 m NH_4OH was 180 – 200 μm/day. Obviously, an increase in the proportion ammonia in solution leads to an increase in the rate of malachite crystallization and an increase in the size of its crystals (table 1).

Table 1. Crystal sizes of synthetic malachite obtained in solutions 0.2 – 2.5m NH_4OH

Solution concentration NH_4OH, mol/kg	0.2 m	0.5 m	2.0 m	2.5 m
Crystal sizes (in diameter), μm	0.2 – 0.4	4 – 8	8 – 15	20 – 25

The crystals of prismatic habit in malachite aggregates are usually isometric. The edges of crystals are smoothed, the surface of the crystals face are rough. In samples of the banded synthetic malachite with contrasting color zoning, there is a change arrangement of aggregates in differently colored color zones. On fig. 2 a (lower and upper part of the figure, visually dark green layer) it is clear that the crystals are located perpendicular to the horizontal surface of crystallization, light green zone - under angle to them (middle part). The same regularity is observed in natural malachite. Crystals in samples of malachite (DR Congo) banded texture with parallel layers of contrast coloring crystals of the light green zone are arranged vertically (lower part of the figure), dark green (upper part of the figure) - at an angle to the crystallization front (Fig. 2b). More than 30 samples of Congolese malachite of banded textures were studied. Most of the samples are composed of parallel columnar aggregates. Crystals in aggregates have a prismatic habit, some of them are flattened. As seen in figures 2b, c, the crystal sizes of the presented samples differ significantly: from 4 - 7 to 20 - 25 microns in thickness.

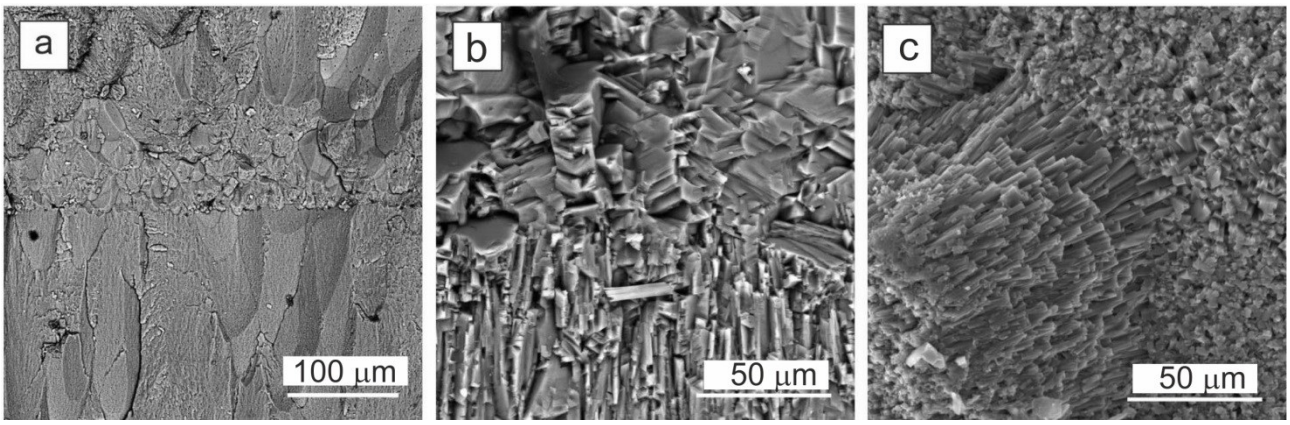

Fig.2 SEM images of samples: a - synthetic malachite grown in a solution of 2.5 m NH_4OH; b, c – malachite is present, from the Kolwezi deposit (DR Congo).

Present studies have shown that the sizes of crystals, as in synthetic, and in natural malachite of a banded texture, can differ significantly. The concentration of the crystallization solution, in our case, ammonium hydroxide, has a major influence on the formation of aggregates during the synthetic malachite crystallization. An increase in the concentration of solutions leads to an increase in the equilibrium concentration copper in solution and increase the rate of crystallization of malachite. It is shown that the sizes of individuals in aggregates of malachite synthesized in highly concentrated solutions significantly exceed those in samples malachite obtained in low-concentration solutions. Differences in the size of crystals from aggregates of natural malachite are possible with a change in the chemical conditions of the process of its crystallization, i.e. with an increase or a decrease in the concentration of the main components of the mineral-forming solution - copper and carbon dioxide.

This study is fulfilled under Research program № FMUF-2022-0002 of the Korzhinski Institute of Experimental Mineralogy

References

Bublikova T.M., Balitsky V.S., Timokhina I.V. Synthesis and main properties of jewelry and ornametal malachite. Synthesis of minerals. V. 1. Alexandrov, VNIISIMS. 2000. 662 p. (In Russian).

Bublikova T.M., Balitsky V.S., Setkova T.V. Study of basic copper carbonate solubility in aqueous ammonia solutions (theoretical and experimental data) // Experiment in GeoSciences. 2013. V.19, No.1. P.74 – 75.

Grigor'ev D.P. On the genesis of speleothems or metacolloid collomorphic aggregates of minerals, Zap. Vseross. Min. O-va, 1953, V. 82, No. 1, pp. 7–22.

Mukendi, E.B., Criteria of the geological–commercial assessment of malachite from the Democratic Republic of the Congo, Cand. Sci, (Geol.-Min.) Dissertation, Moscow: Mosk. Geol.-Razved. Inst., 2009.

Semenov, V.B., Malakhit (Malachite), Sverdlovsk: Sredneuralsk.Kn. Izd., 1987, V. 1–2.

Chernenko, T.V. and Mel'nikov, E.P., Properties and diagnostics of natural and synthetic malachite, Vestn. Gemmol., 2003, nos. 8–9, pp. 11–26.

Shuyskiy, A.V., Experimental mineralogy and genesis of synthetic malachite, Cand. Sci. (Geol.-Min.) Dissertation, St. Petersburg: St. Petersburg Gos. Univ., 2015.

Kovalev V. N.[1], Spivak A. V.[2], Setkova T. V.[2], Borovikova E. Y.[1], Zakharchenko E. S.[2] Raman spectroscopy of $Si_{1-x}Ge_xO_2$ solid solution with α-quartz structure at pressure up to 30 GPa. UDC: 543.42; 549.514.51

[1] Faculty of Geology, Lomonosov Moscow State University, Moscow, Russia kovvn99.msu16@gmail.com, amurr@mail.ru; [2] D.S. Korzhinskii Institute of Experimental Mineralogy of Russian Academy of Sciences (IEM RAS),Chernogolovka, Moscow District, Russiaemail: spivak@iem.ac.ru setkova@iem.ac.ru

Abstract. Spontaneous α-$Si_{1-x}Ge_xO_2$ single crystals with germanium content x = 0.092 and x = 0.195 were studied by Raman spectroscopy at pressure up to 30 GPa. Under standard conditions there is a shift of vibrational modes to a lower frequency region with an increase in the germanium content. There is a shift of vibrational modes to a higher frequency region with increasing pressure. Experimental data suggests a polymorphic transition in α-$Si_{1-x}Ge_xO_2$ crystals at ~11 GPa for x = 0.092 and at ~10 GPa for x = 0.195. An increase in the germanium content lowers the pressure of a possible polymorphic transition.

Keywords: Raman spectroscopy, hydrothermal synthesis, high pressure, germanium, quartz

High-germanium quartz (HGQ) from chemical point of view is a solid solution described as $Si_{1-x}Ge_xO_2$. Crystals of this compound are α-quartz-like, i.e., their structure can be represented as a distorted quartz structure. HGQ single crystals are prospective piezoelectric material with higher values of piezoelectric constants (for instance, piezoelectric modules d_{11} and e_{11}) in comparison with a pure (non-germanium) quartz. In contrast to other quartz-like piezoelectric materials, simple and safe technique for α-$Si_{1-x}Ge_xO_2$ hydrothermal synthesis has been developed. Fluoride solutions proved to be more effective in their synthesis (Balitsky et al., 2004). Spectroscopy study of α-$Si_{1-x}Ge_xO_2$ crystals in wide range of temperatures and composition demonstrated a linear dependence between α→β transition temperature and germanium content. As a result, piezoelectric α-modification becomes thermally stable at high temperatures with increasing germanium content. The features of Raman spectra of α-$Si_{1-x}Ge_xO_2$ crystals with various germanium content under high temperatures were also determined. The shift of vibrational modes to the lower frequencies region with increasing germanium content and temperature was noted (Ranieri et al., 2009).

Along with that, α-$Si_{1-x}Ge_xO_2$ single crystals have not been studied under high pressures. This is a separate relevant research issue. Polymorphic transitions at high pressures were studied *in situ* only for solid solution endmembers SiO_2 and GeO_2 (fig.1).

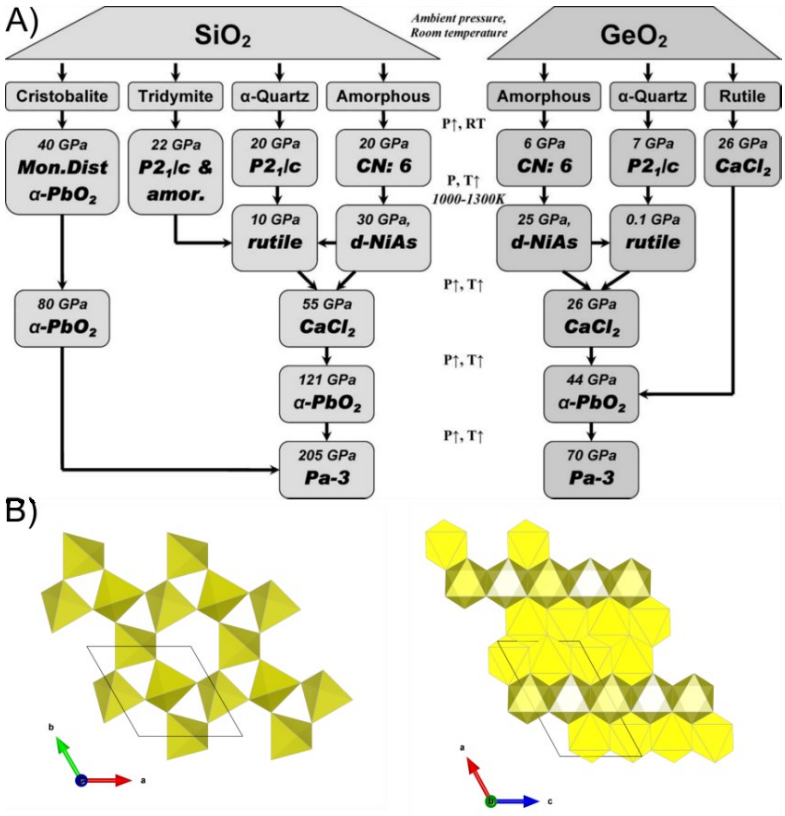

Fig.1 A) Polymorphic transitions of SiO_2 and GeO_2, depending on the PT-conditions and substrate type (Prakapenka et al., 2004). B) Crystal structures of α-quartz (left subfigure) and high-pressure SiO_2 phase with space group $P2_1/c$ (right subfigure). In the structure of high-pressure phase partially occupied octahedra M1 and M2 (transparent) and fully occupied octahedra M3 (yellow) are indicated.

For α-SiO_2 and α-GeO_2 (quartz-like) polymorphic transition «α-quartz-$P2_1/c$» occurs at 20 GPa and 7 GPa at room temperature, respectively. Structure of high-pressure phase can be described as of 3 x 2-kinked chains of edge-sharing GeO_6 octahedra. Chains are stretched along *a* axis. Unit cell parameters: a = 8.285 Å, b = 4.320 Å, c = 5.410 Å, β = 119.94. M1 and M2 positions are partially occupied, M3 position is fully occupied (Haines et al., 2000).

Described experimental results provide to suggest the correlation between solid solution composition and the value of pressure of polymorphic transition mentioned above. In this regard, high pressure study of solid solution single crystals with a certain composition is of interest.

Germanium-bearing quartz crystals were synthesized in autoclaves by hydrothermal temperature-difference method at temperature 600/650°C and pressure 100 MPa. Boric acid solution (30 wt.% H_3BO_3) was taken as a mineralizer. Duration of experiment is 3 weeks. Spontaneous quartz crystals up to 2.5 cm in size were obtained (fig.2).

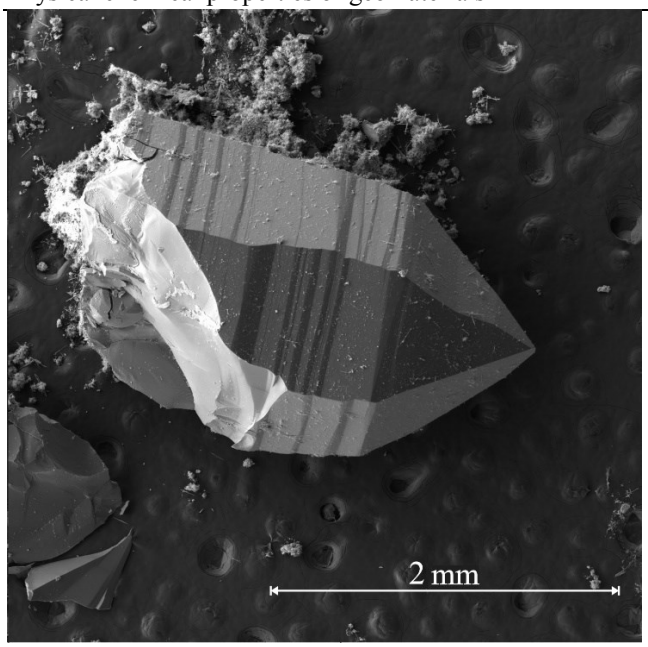

Fig.2 SEM-image of typical well-faceted spontaneous α-$Si_{1-x}Ge_xO_2$ single crystal.

Their composition was studied with scanning electron microscope scanning electron microscope Tescan Vega II XMU (Tescan, Czech Republic), equipped with an INCA Energy 450 X-ray spectral microanalysis system with energy dispersive (INCA Xsight) and crystal diffraction (INCA Wave 700) X-ray spectrometers (Oxford Instruments, England) and the INCA Energy+ software platform. SiO_2 ($Si–K_a$) and germanium metal ($Ge–L_a$) were used as standards for the elements.

The determined composition of selected single crystals corresponds to α-$Si_{0.91}Ge_{0.09}O_2$ и α-$Si_{0.80}Ge_{0.20}O_2$. The germanium distribution in these crystals is uniform.

Structural features of solid solution single crystals under the pressure were studied by Raman spectroscopy. The spectra were recorded *in situ* in the back-scattering geometry using Raman setup comprised of spectrograph Acton SpectraPro-2500i, Olympus BX51 microscope and a Pixis2K CCD detector system cooled to -70°C. The laser beam (wavelength 532 nm) was focused on the sample by 50x objective in a spot with diameter of 5 μm. The signal acquisition time was 720 sec (3 x 240 sec). Measurement of Raman spectra were carried out using Mao-Bell type diamond anvil cell (fig.3). Sixteen-faceted diamond anvils with 250 μm culet were used. NaCl was used as a pressure transmitting medium and the ruby fluorescence technique was used for pressure calibration. α-$Si_{1-x}Ge_xO_2$ single crystals fragments were used as a sample with typical dimensions of ~30 μm.

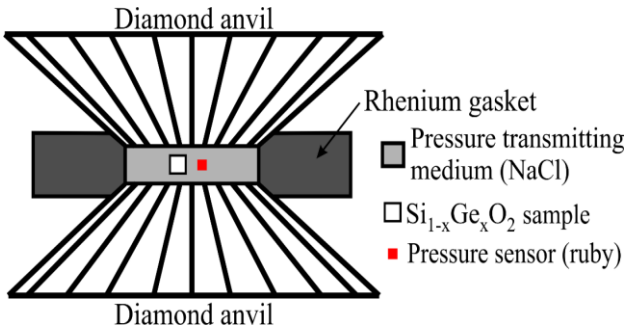

Fig.3 The loading of diamond anvil cell for *in situ* Raman spectroscopy study at high pressures.

Group theory predicts 12 active Raman modes in α-SiO_2 и α-GeO_2 spectra (S.G. $P3_121/P3_221$, factor-group D_3). 4 of them are non-degenerate (A_1) and 8 – twice degenerate (E). Under standard conditions of the 12 expected modes 10 modes (4 – A_1, 6 – E) in α-$Si_{0.91}Ge_{0.09}O_2$ и α-$Si_{0.80}Ge_{0.20}O_2$ Raman spectra were observed (table 1).

Distinction between numbers of determined and predicted by group theory vibration modes can be explained by structural distortions occurring under Si→Ge isomorphism in quartz structure. These distortions contribute to the shift of Raman spectra vibration modes relative to the solid solution endmembers. There is a shift of vibrational modes to lower frequencies region with increasing germanium content what agrees with (Ranieri et al., 2009; Koshchug et al., 2020).

Table 1. Active modes position in Raman spectra of α-$Si_{0.91}Ge_{0.09}O_2$, α-$Si_{0.80}Ge_{0.20}O_2$ samples and solid solution endmembers.

Sample composition	Peak position (cm^{-1}) and vibration type									
	A_1	A_1	A_1	A_1	E	E	E	E	E	E
α-SiO_2*	206	356	465	1083	128	509	697	795	807	1160
α-$Si_{0.91}Ge_{0.09}O_2$	225	399	469	1016	137	580	643	747	810	1147
α-$Si_{0.8}Ge_{0.2}O_2$	219	399	464	1002	133	569	632	743	806	1136
α-GeO_2*	212	261	440	880	121	456	512	583	595	961

Note: * - Raman spectra according to (Scott, 1970).

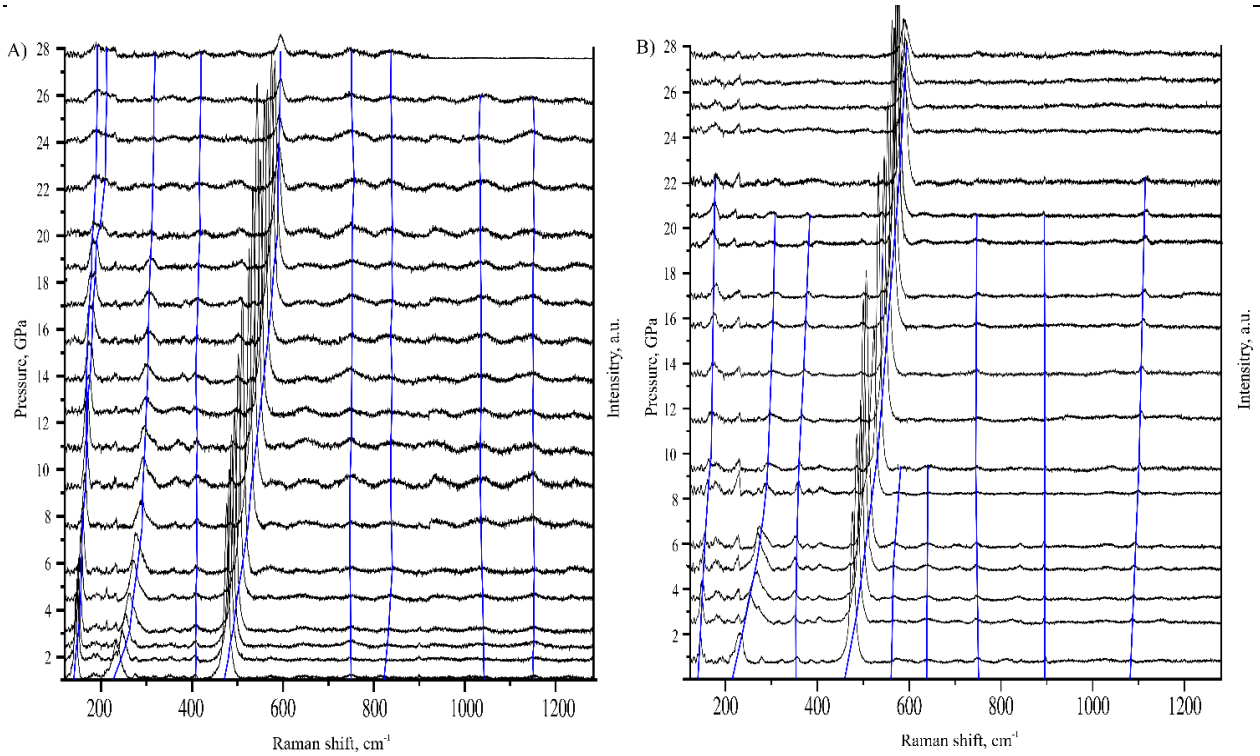

Fig.4 Raman spectra of α-$Si_{0.91}Ge_{0.09}O_2$ (A) and α-$Si_{0.80}Ge_{0.20}O_2$ (B) under pressure. Blue lines are trend lines that show a shift of vibrational modes.

Raman spectra of α-$Si_{0.91}Ge_{0.09}O_2$ и α-$Si_{0.80}Ge_{0.20}O_2$ under pressure are on fig.4. The general trend – the shift of vibrational modes to higher frequencies region with increasing pressure is noticed. This trend is more noticeable for the most intensive modes.

Bands with wave numbers 137 (E) and 225 cm^{-1} (A_1) correspond to complex deformation vibrations of the silicon-germanium oxygen framework (Koshchug et al., 2020). When the pressure increases to ~ 11 GPa, these bands monotonically shift to values of 161 and 288 cm^{-1}, respectively. At a pressure of > 11 GPa, the slope of the trend lines changes, after which the monotonous growth continues. Also, at 11 GPa, the band (137 cm^{-1}) degenerates to form a pair of LO-TO, 161 and 165 cm^{-1}, respectively. The LO band monotonically increases to 184 cm^{-1} at 28 GPa. At the same time, the current band at 22 GPa takes the value 204 cm^{-1}, and with a subsequent increase in pressure becomes indistinguishable. For the A_1 band at a pressure > 11 GPa, a monotonous growth continues to 303 cm^{-1} at a pressure of ~ 20 GPa, after which this vibration band becomes indistinguishable.

The 469 cm^{-1} (A_1) band corresponds to O-(Si/Ge)-O deformation vibrations (i.e., a change in the angle θ) (Koshchug et al., 2020). This band is characterized by a monotonous growth up to 536 cm^{-1} at 11 GPa, after which the direction of the trend line changes. With the subsequent increase in pressure, the position of the strip gradually shifts to 589 cm^{-1} at 28 GPa. The 469 cm^{-1} band is also characterized by the presence of a shoulder at 445 cm^{-1}, which at ~ 5-6 GPa stands out as a separate peak.

The change in the slope of the trend lines of the main bands of the Raman spectra (225 and 469 cm^{-1}), the bifurcation (137 cm^{-1}) and disappearance (580 cm^{-1}) of the lines at a pressure of ~ 11 GPa suggests a polymorphic transition of the $Si_{0.91}Ge_{0.09}O_2$ solid solution at this pressure value.

The α-$Si_{0.80}Ge_{0.20}O_2$ crystal is characterized by similar changes in the Raman spectra with increasing pressure, the differences are only quantitative. The bands 219 cm^{-1} (A_1) and 133 cm^{-1} (E) monotonically shift to the wave numbers of 285 cm^{-1} and 159 cm^{-1}, respectively, at a pressure of ~10 GPa, after which the direction of the trend line changes. The 464 cm^{-1} vibrational band shifts up to 530 cm^{-1} at a pressure of ~ 10 GPa. with subsequent pressure increase, the slope of the trend line changes, and monotonous growth continues. At this pressure value (~10 GPa) it is possible to notice the disappearance of the vibrational bands with wave numbers 637 cm^{-1} and 569 cm^{-1}. Thus, it is possible to assume the above polymorphic transition at a pressure value of ~ 10 GPa.

Experimental data provide to conclude that the polymorphic transition pressure value decreases with increasing germanium content in $Si_{1-x}Ge_xO_2$ single crystal (table 2). Germanium, as a larger cation, contributes to structural distortions with the isomorphic substitution. As a result, a sharp decrease in pressure value is noted. It can be seen by changing pressure value of α-$Si_{0.91}Ge_{0.09}O_2$ relative to pure quartz. With a further increase in germanium content the dependence becomes linear.

Table 2. Dependence of «α-quartz-$P2_1/c$» polymorphic transition pressure value on solid solution composition.

Sample composition	α-SiO_2*	α-$Si_{0.91}Ge_{0.09}O_2$	α-$Si_{0.8}Ge_{0.2}O_2$	α-GeO_2*
P, GPa	20	11	10	7

Note: * - pressure values according to (Prakapenka et al., 2004)

The study is fulfilled under Research program FMUF-2022-0002 of the Korzhinskii Institute of Experimental Mineralogy.

References

1. Balitsky V.S., Balitsky D.V., Nekrasov, A.N., Balitskaya L.V., Bondarenko G.V., Samokhvalova O.L. Growth, structural-morphological features, and some properties of quartz-germanuim oxide solid solution single crystals with quartz structure. // Doklady Earth Sciences. 2004. 396. 500-503.
2. Haines J., Leger J.M., Chateau C. Transition to a crystalline high-pressure phase in α-GeO_2 at room temperature // Physical Review B. 2000. 61. pp. 8701–8706.
3. Koshchug D.G., Koshlyakova A.N., Balitsky V.S., Vyatkin S.V. Infrared and Raman spectroscopy study of $Si_{1-x}Ge_xO_2$ solid solutions with α-quartz structure // Spectrochimica Acta Part A: Molecular and Biomolecular Spectroscopy. 2020. 233. 118168.
4. Prakapenka V.P., Shen G., Dubrovinsky L.S., Rivers M.L., Sutton S.R. High pressure induced phase transformation of SiO_2 and GeO_2: difference and similarity // Journal of Physics and Chemistry of Solids. 2004. 65. pp. 1537–1545.
5. Ranieri V., Bourgogne D., Darracq S., Cambon M., Haines J., Cambon O., Leparc R., Levelut C., Largeteau A., Demazeau G. Raman scattering study of α-quartz and $Si_{1-x}Ge_xO_2$ solid solutions // Physical Review B. 2009. 79. 224304.
6. Scott J.F. Raman Spectra of GeO_2 // Physical Review B. 1970. 1(8). pp.3488-3493.

Kuleshova M.L.[1], Danchenko N.N.[2], Shimko T.G.[1] Experimental evaluation of the immobilizing capacity of clay materials as geochemical barriers for radionuclides.

[1]Geological Faculty of Moscow State University, Moscow
[2]V.V. Dokuchaev Soil Science Institute, Moscow e-mail: rita5715@mail.ru

Abstract. Assessment of effectiveness of natural clay grounds and commercial mixtures on their basis as materials for engineering barriers in sites of storage and disposal of radioactive waste (RW) is an urgent task of modern geoecology. The purpose of the present study was to determine the most effective barrier materials in relation to RW components among available clay mixtures and common grounds of different composition. The objects of the study were ferruginous clay, kaolin loam, bentonite of PBMV grade and a mechanically activated mixture of bentonite, kaolinite and vermiculite (MAC mixture). The test solution contained a number of elements whose radioactive isotopes or analogs are the main components of RW of hazard class III and IV. Experimental determination of potential immobilizing ability characteristics and sorption parameters in static mode showed that the studied materials by their efficiency are as follows: 1) PBMV bentonite; 2) MAC mixture; 3) ferruginous clay; 4) kaolin loam. Immobilizing ability of ferruginous clay for some elements was higher than that of MAC mixture.

Keywords: clay materials, radionuclides, immobilization, distribution coefficients

Introduction

The study of the effectiveness of natural clay soils and industrial mixtures based on them, as available materials for engineering safety barriers (ESB) in places of storage and disposal of radioactive waste (RW), is today an urgent task of geoecology. Depending on the immobilizing ability, filtration and a number of other characteristics of materials, they can be used both to create external insulation of storage facilities and to fill the internal space of such structures. In some cases, economic feasibility at a particular disposal site dictates the study of local clay soils for the construction of such ESBs. Information on the interaction of specific clay materials with radionuclides is important in the development of general knowledge on this issue, it is included in databases on clay materials as ESB materials, and is used in the design of radioactive waste disposal facilities.

Materials and research methods

The purpose of this work is to conduct a comparative assessment of the effectiveness of a number of natural clay soils and artificial barrier mixtures in relation to the components of radioactive waste of III and IV hazard classes. Five samples were included in the experimental series: Fe-rich clay, loam (kaolin), bentonite grade PBMV of the Zyryanskoye deposit, and a mechanically activated composite mixture consisting of bentonite, kaolinite and vermiculite (MAC mixture). Studies were carried out on stable isotopes of Cs and Sr; low-activity isotopes U-238 and Th-232, stable elements-simulators of radionuclides Ba (analogue of Ra-226), Nd and Dy (analogues of Am-241, Cm-244), Re (analogue of Tc-99). The justification for the validity of such a set of elements as analogues of radionuclides for model experiments is given in (Sergeev et al., 2009).

For a general characterization of the selected materials, the granulometric and mineral composition, as well as the cation exchange capacity (CEC) were determined. Granulometric analysis was carried out according to GOST 12536-2014. The

mineral composition was determined by X-ray phase analysis using a RIGAKU MULTIFLEX 600 diffractometer. CEC was determined by the Antipov-Karataev and Mamaeva method modified by Zlochevskaya. The results are shown in table 1.

Table 1. The main characteristics of the samples that determine their sorption properties

Sample	Faction content <0,01mm, %	The content of sorbing minerals, %						CEC mg eq/100 g
		smectite+ mixed-layer minerals	vermicu-lite	kaolinite	hydromica	goethite	calcite	
Fe-rich clay	58	2+9	-	4	4	13	-	24
Kaolinite loam	26	-	-	53	0,8	-	-	8
Bentonite PBMV	92	72	-	1	5	-	4	110
MAC mixture	85	51+7	30	10	1	-	3	30

Based on the characteristics obtained, it could be expected that bentonite has the best potential ability to immobilize elements due to the high content of smectites and physical clay. The extremely high CEC value for it is associated with alkaline processing of the original natural raw materials. MAC mixture is similar in properties to bentonite, but somewhat worse than it. The presence of calcite in samples of bentonite and MAC mixture can adversely affect the absorption of uranium, since uranyl carbonate complexes are very stable (Vdovenko, 1960), especially in alkaline solutions (Semenkova et al., 2021). Clay can be a good sorbent due to the smectite component, a fairly high content of physical clay (58%), and the presence of ferruginous minerals (goethite - 13%). According to the studied characteristics, kaolin loam is the least effective for absorbing radionuclides.

To prepare a model polyelement solution, salts of the above listed elements of the "chemically pure" qualification were used, as well as a model solution imitating atmospheric water filtered through clay overlying deposits, of the following macrocomponent composition (mg/l): Na - 68; Mg - 7; Ca - 7; HCO_3 - 186; Cl - 11; SO_4 - 10; pH 6.65.

The absorption capacity was evaluated in static mode. A sample of clay material was balanced with polyelement solutions of salts of the following concentrations (for each element): 0.01 mg/l; 0.1 mg/l; 1.0 mg/l; 10.0 mg/l. The ratio of sorbent:solution was 1:100. The exposure time sufficient to achieve equilibrium - 1 day - was determined on the basis of a preliminary study of the kinetics of the sorption process. After equilibration, the concentration of all the studied elements in aliquots of the initial and equilibrium solution was determined by ICP-MS and sorption isotherms were plotted.

Results and discussion

The adsorption isotherms in the studied concentration range for most elements were linear, with the exception of Th, which is extremely prone to hydrolysis and polymerization. Immobilization for him is mainly due to sedimentation. Typical isotherms on the example of Fe-rich clay are shown in fig. 1.

Based on the data of isotherms for all materials, the distribution coefficients (K_d) between the solution phase and the sorbent were determined (Fig. 2), which give a visual representation of the severity of the barrier properties of materials. As can be seen from the figures, the efficiency of immobilization is significantly higher for transition elements - rare earths Nd and Dy, as well as Th, whose ions are easily polarizable and can more easily reach the charged surface of the mineral phase.

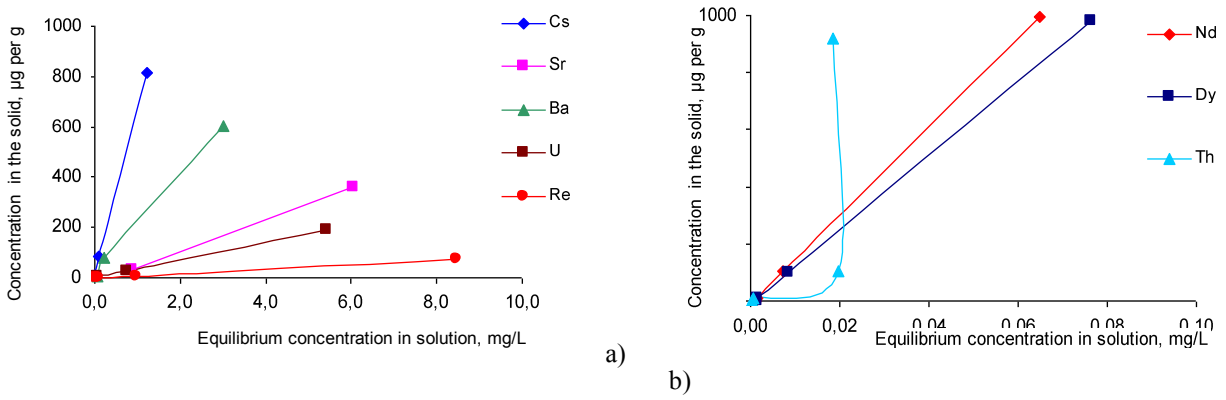

Fig. 1. Adsorption (immobilization) isotherms on a ferruginous clay sample: a) weakly hydrolysable ions (group I); b) ions prone to hydrolysis (group II).

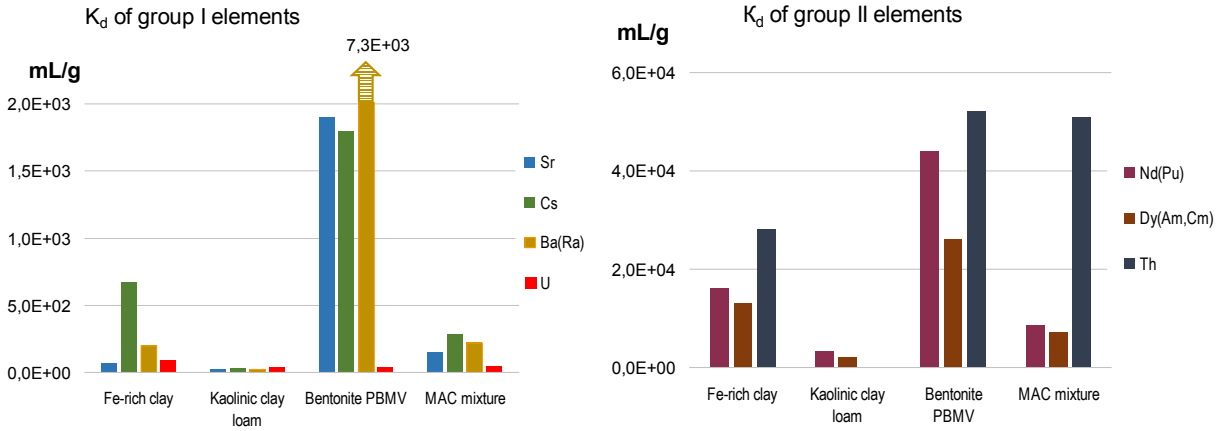

Fig. 2. Distribution coefficients between the sorbent material and the solution for ions of elements of groups I and II.

Polarizability also determines their high tendency to hydrolysis, which provides a significant contribution of the deposition process to their immobilization. The minimum absorption was observed for Re, which in aqueous media (as well as for Tc) exists mainly in the form of the ReO_4– oxoanion. Any noticeable immobilization of Re occurs only on ferruginous clay (K_d = 9 ml/g), which is most likely due to the presence of authigenic Fe films on the surface of clay particles, imparting a partial positive charge to it. In this regard, the diagrams (K_d) do not show data on Re. All clay materials poorly remove U, which is obviously due to the fact that the main form of its existence in aqueous solutions is the very bulky oxocation UO_2^{2+}, as well as the already noted stability of its carbonate complexes in an alkaline medium, and all the studied materials alkalinize the liquid phase. pH of equilibrium solutions in contact with ferruginous clay was 7.7-8.2; kaolinic loam - 7.5-7.6; bentonite - 10.4-10.6; MAC with a mixture of -7.9-8.5 (pH decreased with an increase in the concentration of elements in the contact solution). The described trends appeared for all studied materials. Sufficiently low absorption of Sr, observed for all barrier materials except PBMV bentonite, is associated with competition with Ca, which is present in a significant concentration in the model solution. The distinctive high efficiency of Sr binding by PBMV bentonite is probably due to its high dispersity and high CEC - indicators that this bentonite acquired as a result of special alkaline treatment.

In terms of K_d values, the studied materials form the following decreasing series: Bentonite PBMV >> MAC mixture > Ferroclay >> Kaolin loam. At the same time, the immobilizing ability of ferruginous clay for a number of elements (Cs, Nd, Dy) turned out to be higher than that of the MAC mixture.

Despite the large differences in K_d, the specific absorption capacity (N) in moles per gram differs little both for different elements on the same material and for the same element on different materials (Table 2). This fact, apparently, is due to the fact that in the studied range of initial concentrations, the limiting absorption capacity is not achieved for any of the elements on any sample.

The immobilization potential of the studied materials with respect to the components of the multi-element test solution is well illustrated by the data in Table. 3.

Table 2. Specific absorption capacity of barrier materials in relation to the components of a multi-element solution at an initial concentration of 1 mg/l.

Element-sorbate	Specific absorbency, mol/g			
	Fe-rich clay	Kaolin loam	Bentonite PBMV	MAC mixture
Sr	3E-07	3E-07	1E-06	3E-07
Cs	6E-07	2E-07	7E-07	5E-07
Ba (Ra)	6E-07	3E-07	7E-07	5E-07
U	1E-07	6E-08	8E-08	9E-08
Nd (Am,Cm)	7E-07	7E-07	7E-07	7E-07
Dy (Am,Cm)	6E-07	6E-07	6E-07	6E-07
Th	5E-07	5E-07	5E-07	5E-07

Table 3. Immobilization of elements (in %) on barrier materials under static conditions at an initial solution concentration of 1 mg/l for each element

Element	Fe-rich clay	Kaolin loam	Bentonite PBMV	MAC mixture
Sr	26	13	94	20
Cs	89	32	96	77
Ba	79	32	97	70
U	18	17	13	13
Nd (≈Dy)	99	96	99	99
Th	98	100	99	100

PBMV bentonite exhibits the maximum cumulative efficiency to the entire studied set of elements. This is consistent with the features of its granulometric (high content of clay fraction) and mineral composition (high content of smectites and mixed layers), as well as a very high CEC value. The ferruginous clay is only slightly inferior to it in terms of the efficiency of removing Cs and Ba, but it removes Sr from the solution noticeably worse. The effectiveness of the MAC mixture is slightly inferior to clay in the 3 listed elements. Kaolin clay is the least effective, which also correlates well with its composition.

Conclusions

The efficiency of radionuclide immobilization on clay soils and bentonite mixtures depends both on the clay material itself and on the type of radionuclides. Of the studied clay samples, PBMV bentonite can be recommended as a material for internal ESB in storage sites for class III and IV radioactive waste containing the studied elements. Ferruginous clay and MAC mixture can also serve as a material for a safety barrier. At the same time, their relatively low sorption capacity for Sr can be compensated by the short half-life of this nuclide, due to which, with a low permeability of the barrier, there will be no release of radioactive strontium beyond the barrier boundaries. With a high probability of leaching of noticeable amounts of uranium from RW, none of the studied materials can be a reliable ESB, which must be taken into account when designing safety measures. Also, clay materials are not capable of absorbing anion-forming elements, such as in this case Re.

In order to assess all acting factors at the radioactive waste disposal facility, it is necessary to carry out mathematical modeling of radionuclide migration in engineering barriers. Depending on the tasks to be solved at a specific facility, the obtained sorption parameters (Kd) can be used in mathematical modeling of the mass transfer of radionuclides both inside the disposal module and on the outer contour of the facility.

Source of funding: state budget topic "Theoretical and experimental study of the influence of geological and technogenic factors on the safety of economic activity" within the framework of the priority scientific direction "Geological support of the mineral resource base, safety of economic activity and infrastructure development in Russia" of the NP of Russia "Rational nature management". CITIS: AAAA-A16-116033010108-8

References

1. Vdovenko V.M. Chemistry of uranium and transuranic elements. Publishing House of the Academy of Sciences of the USSR, M.-L., 1960, 700 p. *(in Rus.)*
2. Semenkova A.S., Il'ina O.A., Krupskaya V.V., Zakusin S.V., Dorzhieva O.V., Pokidko B.V., Romanchuk A.Yu., Kalmykov S.N. Sorption of radionuclides on clay minerals-components of engineering safety barriers // Bulletin of Moscow State University. Series 2: Chemistry. 2021. V.62. No. 5. pp. 425-434 *(in Rus.)*

3. Sergeev V.I., Danchenko N.N., Kuleshova M.L. Evaluation of the effectiveness of sand-gel material as a sorption screen on the path of migration of radionuclides //Voprosy atomnoi nauki i tekhniki. Series: Physics of nuclear reactors. 2009. No. 1. P. 42–48 *(in Rus.)*

Tselmovich V.A.[1], Doronicheva E.V.[2] Microstructure and composition of flint artifacts from layers 7 and 8 in Sosruko grotto in the Elbrus region. UDC: 620.187; 550.4

[1] Borok Geophysical Observatory, the Branch of Schmidt Institute of Physics of the Earth, Russian Academy of Sciences, Borok, Yaroslavl region, 152742 Russia tselm@mail.ru,

[2] Laboratory of Prehistory, 6M Liflandskaya str., 6M, 215, St.-Petersburg, 190020, Russia

Abstract. We have studied a sample of 18 flint artifacts from different horizons of layers 7 and 8 (13-16 kya) in Sosruko grotto, located in the Elbrus region. Data on morphology and chemical composition was obtained using an Olympus BX-51 metallographic microscope and a Tescan Vega II scanning electron microscope with a device for energy dispersive analysis. Our research shows that optical microscopy indicates structural and textural inhomogeneities associated with flint formation. The morphology of all samples looks similar at a low magnification, but differs markedly at a high magnification due to the presence of various inclusions. The data was correlated with the previously obtained results for flint outcrops in the region. On the basis of this research we make suggestions about possible flint sources that were exploited by Epipaleolithic hunter-gatherers in different periods of the site occupation.

Keywords: Scanning electron microscopy; flint artifacts; Epipaleolithic; Sosruko grotto; Caucasus.

Introduction. The reconstruction of lithic raw material strategies is an important topic in the study of human adaptations in the Paleolithic. The main raw materials for the manufacture of tools in that period were different types of rocks, most often flint, which is widespread in the nature. Research addressed to the study of exploitation of different types of stone raw materials, reconstruction of paths and distances that human groups overcame for the procurement of local or exotic raw materials, methods of their transportation are actively carried out in different regions of Eurasia (e.g.., Doronicheva, 2011; Doronicheva, Kulkova, 2016, Ekshtain et al. 2014; Frahm et al., 2016; Sánchez de la Torre et al. 2020).

The purpose of this research was to study, using optical and scanning electron microscopy, a selection of flint artifacts from layers 7 and 8 in Sosruko grotto in the Elbrus region (Zamyatnin, Akritasd, 1957; Golovanova et al., 2019; 2020), and to determine the flint sources , which could be used by humans that occupied the site in different periods. The 18 artifacts from different horizons were analyzed and the data was compared with the previously obtained data on flint outcrops in the North Caucasus. The research allowed us to draw some new conclusions about human mobility during the Epipaleolithic period (13-16 thousand years ago) in the North Caucasus.

Materials and methods. The study of thin sections of flints was carried out first on an optical microscope and then using the microprobe analysis on a scanning electron microscope. The optical microscopy showed a great variety in color of the studied objects; red and dark red colors predominated. The microprobe studies have shown that the coloration is caused by various iron oxides and hydroxides, which differed both in the oxidation degree and the size of micro- and nanoparticles.

The chemical composition was determined based on EDS spectra in weight percent. For calibrations in a quantitative analysis, certified reference samples of synthetic crystals and natural minerals were used. The spectra were processed using the INCA software package (Oxford Instrument Analytical Ltd.).

Results and discussion. All flint samples studied with the optical microscopy can be divided into two groups according to their structural and textural features: 1) in the aphanite transparent colorless matrix there are large magnetite phenocrysts (porphyritic structure; Fig. 2-1); 2) an opaque banded matrix with a fluid texture (Fig. 2-2). In some samples, both structural-textural types are found.

Sample No. 1-2020-KB. SSR-2019, l.8, h.9, No. 45. Rock color: light grey. Characteristic minerals: quartz, calcite, faunal remains. Structure: porphyroclast. Pyrite is absent.

Sample No. 2-2020-KB. SSR-2019, l.8, h.6, No. 199. Rock color: light gray. Characteristic minerals: quartz, calcite, faunal remains. Structure: porphyroclast. Texture: fluid, mottled.

Sample No. 3-2020-KB. SSR-2019, l.7, h.2, No. 97. Rock color: light grey. Characteristic minerals: quartz, calcite, faunal remains. Structure: porphyroclast. Texture: fluid, mottled. Hematite microsphere in a pore. Pyrite is absent.

Sample No. 4-2020-KB. SSR-2019, l.8, h.11, No. 131. Rock color: light beige. Characteristic minerals: apatite, quartz, remains of fauna with a small admixture of calcium. Structure: porphyroclast. Texture: mottled.

Sample No. 5-2020-KB. SSR-2019, l.8, h.7, F-10, No. 5601. Rock color: light beige. Characteristic minerals: quartz, apatite, small impurities and calcite, faunal remains with 100 nm pores. Structure: afanite. Texture: spotted.

Sample No. 6-2020-KB. SSR-2019, l.8, h.11, No. 83. Rock color: light beige. Structure: homogeneous with few pores. A magnetite ball was found in one of the pores. Texture: spotted.

Sample No. 7-2020-KB. SSR-2019, l.8, h.11, No. 163. Rock color: light grey. Characteristic minerals: quartz, calcite, apatite, faunal remains. Structure: porphyroclast. Texture: spotted.

Sample No. 8-2020-KB. SSR-2019, l.8, h.5, No. 420. Rock color: light beige. Characteristic minerals: quartz, calcite, faunal remains. Structure: afanite. Texture: spotted.

Sample No. 9-2020-KB. SSR-2019, l.8, h.6, No. 12. Rock color: light grey. Characteristic minerals: quartz, apatite, few faunal remains of fauna. Structure: amorphous. Texture: friable, spotted.

Sample No. 10-2020-KB. SSR-2019, l.8, h.11, No. 111. Rock color: light beige. Characteristic minerals: quartz, faunal remains. Structure: porphyroclast. Texture: spotted, porous.

Sample No. 11-2020-KB. SSR-2019, l.8, h.6, No. 187, coal. Rock color: dark pink.

Characteristic minerals: quartz, calcite, apatite, faunal remains. Structure: porphyroclast. Texture: spotted, with numerous calcite lateral inclusions.

Sample No. 12-2020-KB. SSR-2019, l.8, h.11, No. 192. Rock color: light gray-beige. Characteristic minerals: quartz, apatite, faunal remains. Structure: porphyroclast. Texture: spotted with numerous micro- and macropores.

Sample No. 13-2020-KB. SSR-2019, l.8, h.11, No. 158. Rock color: light gray-beige. Characteristic minerals: quartz, calcite (a half of the sample), Fe oxides, ferruginous microspheres (Fig. 13c). Structure: porphyroclast. Texture: spotted, friable.

.

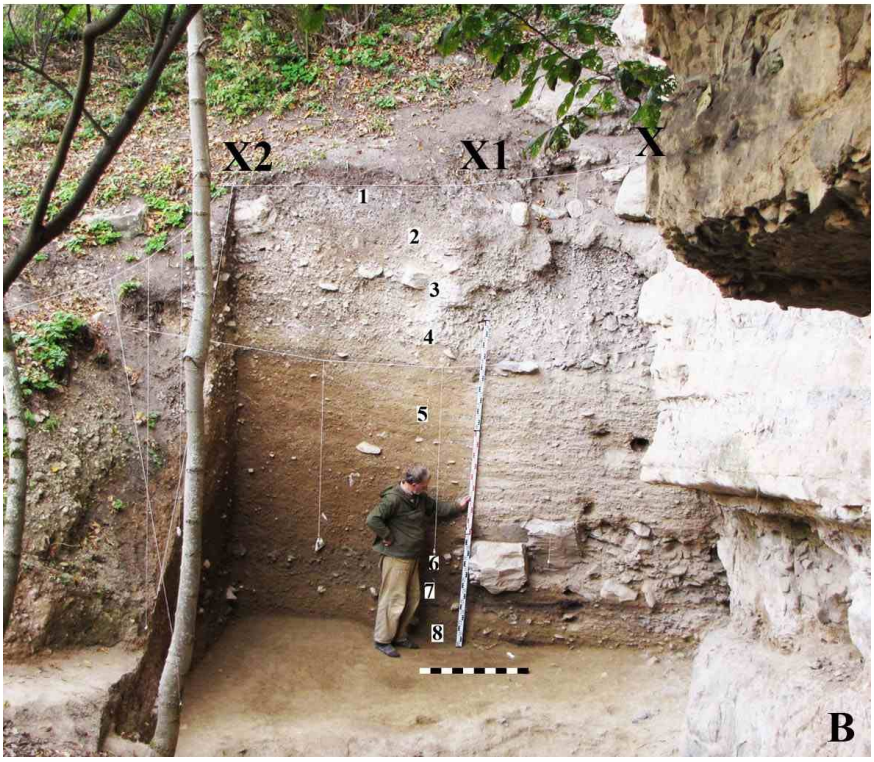

Fig. 1. Paleolithic site in the Sosruko grotto. A. Physical map of Kabardino-Balkarian Republic showing the position of the Sosruko grotto. B. General view of the site and section X2X1X in the Sosruko grotto. After (Golovanova et al., 2020: Fig. 2-B).

Sample No. 14-2020. SSR-2019, l.7, h.2, No. 3. Rock color: light grey. Characteristic minerals: quartz, barite, Fe oxides and hydroxides, faunal remains. Structure: porphyroclast. Texture: spotted, friable.

Sample No. 15-2020-KB. SSR-2017, l.7, h.3, D-9, No. 661. Rock color: light grey. Characteristic minerals: quartz, calcite, Fe oxides and silicates. Structure: porphyroclast. Texture: spotted

Sample No. 16-2020-KB. SSR-2019, l.7, h.1, F-9, No. 318. Rock color: light grey. Characteristic minerals: quartz, calcite, barite; pores are filled with finely dispersed barite. Structure: afanite. Texture: spotted, porous.

Sample No. 17-2020-KB. SSR-2019, l.8, h.5, G-10, No. 5263. Rock color: dark pink. Characteristic minerals: quartz, faunal remains of varying porosity degrees; apatite. Structure: afanite. Texture: spotted.

Sample No. 18-2020-KB. SSR-2019, l.7, h.5, F-10, No. 524. Rock color: light grey.

Characteristic minerals: quartz, calcite at the edges and in pores, barite, faunal remains. Structure: afanite. Texture: spotted.

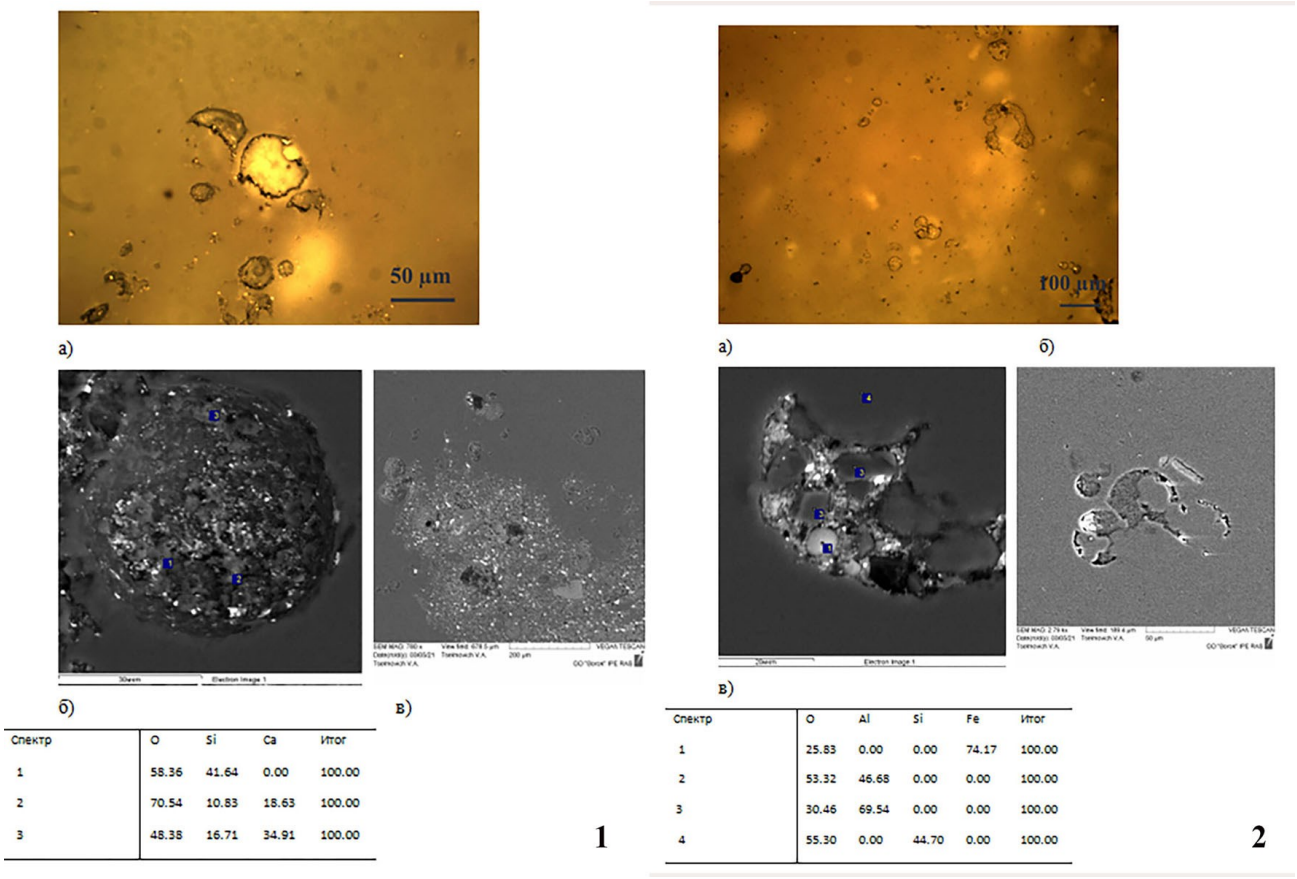

Спектр	O	Si	Ca	Итог
1	58.36	41.64	0.00	100.00
2	70.54	10.83	18.63	100.00
3	48.38	16.71	34.91	100.00

Спектр	O	Al	Si	Fe	Итог
1	25.83	0.00	0.00	74.17	100.00
2	53.32	46.68	0.00	0.00	100.00
3	30.46	69.54	0.00	0.00	100.00
4	55.30	0.00	44.70	0.00	100.00

Fig. 2. 1 – sample 2: a) Olympus BX51 microscope image; b), c) Tescan Vega II SEM images. Characteristic minerals: quartz, calcite, faunal remains. Structure: porphyroclast. Texture: fluid, mottled. 2 - Sample 3: a) Olympus BX51 microscope image; b), c) Tescan Vega II SEM images. Characteristic minerals: quartz, calcite, faunal remains. Structure: porphyroclast. Texture: fluid, mottled. Magnetite microsphere in a pore.

Conclusions. In the result of studies using optical microscopy, inhomogeneities associated with the history of flint formation are distinguished in structural and textural features. Using scanning electron microscopy, morphology of all samples is similar at a low magnification, but differs markedly at a high magnification due to the presence of various inclusions. The chemical composition of the matrix is similar and close to silica in all samples. The specific features of the samples become noticeable in the composition and morphology of microinclusions. Specific inclusions comprise pyrite in the form of membranes and separate particles, or in the form of framboids. Taking into account the redox conditions varied greatly and were characteristic of each sample, a part of pyrite grains was oxidized to magnetite and hematite. Of course, the use of the SEM method for the analysis of stone raw materials should be carried out in combination with other methods, primarily petrography and geochemistry, such as LA-ICP-MS or XRF.

The studies show that most of the samples from layers 7-8 in Sosruko grotto (samples 1-12 and, probably, sample 17) were assigned to the Shtauchukua-1 flint source, located 15-20 km from the grotto in the Baksan River valley. Sample 18

(layer 7, horizon 5) was assigned to the Besleneevskaya flint source, located in a linear distance of approx. 250 km (without accounting the modern relief) in the north-western Caucasus; it additionally confirms contacts of the human population of the Elbrus region with the north-western Caucasus at ca. 13 thousand years ago. Data for some other samples require clarification.

This research was supported by the Russian Science Foundation (grant No. 17-78-20082, "Human-nature interaction in ancient in the Central Caucasus: dynamics of environmental change and technological innovations, and adaptations of subsistence strategies", 2020-2022).

References

Golovanova L.V., Doronichev V.B., Doronicheva E.V. New data about Paleolithic of the Elbrus Region. // Rossiyskaya Arkheologiya. 2019. № 2. P. 7-17.

Doronicheva E.V. Siryeviye strategii drevnego cheloveka v srednem paleolite na Severo-Zapadnom Kavkaze (Raw Material Strategies of Paleolithic Hunter-Gatherers in the North-Western Caucasus Middle Paleolithic). // *Vestnic Sankt-Peterburgskogo Universiteta. 2011. Vol.* 2 (3). P. 192-200.

Doronicheva E.V., Kulkova M.A. Izucheniye kamennogo sirya v paleolite: metodi I rezultati. (Raw material study in the Paleolithic: methods and results). // *Russian Archaeology*. 2016. №2. P. 5-18.

Ekshtain R., Malinsky-Buller A., Ilani S., Segal I., Hovers E. Raw material exploitation around the Middle Paleolithic site of «Ein Qashish». // *Quaternary International*. 2014. Vol. 331. P. 248-266.

Frahm E., Feinberg J.M., Schmidt-Magee B.A., Wilkinson K.N., Gasparyan B., Yeritsyan B., Adler D.S. Middle Paleolithic toolstone procurement behaviors at Lusakert Cave 1, Hrazdan valley, Armenia. // *Journal of Human Evolution*. 2016. Vol. 91. P. 73-92.

Golovanova L.V., Doronichev V.B., Doronicheva E.V., Tregub T.F., Volkov M.A., Spasovskiy Yu.N., Petrov A. Yu., Maksimov F.E., Nedomolkin A.G. Dynamique du climat et du peuplement du Nord-Central du Caucase au tournant du Pléistocène et de l'Holocène. // *L'Anthropologie. 2020.* Vol. 124. Iss. 2. 102759

Sánchez de la Torre M., Utrilla P., Domingo R., Jiménez L., Le Bourdonnec F.-X., Gratuze B. Lithic raw material procurement at the Chaves cave (Huesca, Spain): a geochemical approach to defining Paleolithic human mobility. // *Geoarchaeology*. 2020. P. 1-15.

Zamyatnin S.N., Akritas P.G. Excavation in Sosruko grotto in 1955. *Scientific reports of the Kabardino-Balkarian scientific-research institute. 1957. Vol.* XIII. P. 431–455.